NPL
National Physical Laboratory

Report

NPL REPORT
DEPC-MPE 018

Thermal Diffusivity and Thermal Conductivity Measurements on Oxide Scales

L.A. Chapman, A.T. Fry and S.J. Roberts

NOT RESTRICTED

July 2005

dti
FUNDED BY THE DTI

National Physical Laboratory | Hampton Road | Teddington | Middlesex | United Kingdom | TW11 0LW

Switchboard 020 8977 3222 | **NPL Helpline** 020 8943 6880 | **Fax** 020 8943 6458 | **www.npl.co.uk**

Thermal Diffusivity and Thermal Conductivity Measurements on Oxide Scales

L.A. Chapman, A.T. Fry and S.J. Roberts
Division of Engineering and Process Control

ABSTRACT

This report summarises the methods used to measure the thermal diffusivity of a material using the laser flash technique and demonstrates how the finite difference model "TherMOL", developed at NPL, can be used to evaluate the thermal diffusivity and conductivity of homogeneous single layer materials and multi-layered materials using laser flash data. For the purposes of this report steam oxidised P92 has been used to illustrate how the TherMOL model can separate the thermal conductivities of a substrate and an oxide scale from standard laser flash data.

ISSN 1744-0262

National Physical Laboratory
Hampton Road, Teddington, Middlesex, TW11 0LW

Approved on behalf of the Managing Director, NPL
by Dr M Cain, Knowledge Leader, Materials Processing team
authorised by Director, Engineering and Process Control Division

1 Introduction

This report summarises work conducted as part of the Principles Of Steam Oxidation project, a project in the Life Performance of Materials Programme. The procedures used for the measurement of thermal diffusivity and conductivity of solid oxide scale samples using the Laser Flash technique and the NPL model (TherMOL) are described and examples from measurements conducted on P92 are presented.

The laser flash technique is widely used for the determination of thermal diffusivity. It is capable of yielding results rapidly, on small samples, over a wide temperature range from room temperature (RT) to 1650 °C, and is applicable to a very wide range of materials with diffusivities from $1x10^{-7}$ m^2s^{-1} to $1x10^{-4}$ m^2s^{-1}. This report will demonstrate how the use of such equipment can yield information relating to the thermal diffusivity and how by using NPL developed finite difference modelling routines the thermal conductivity of the oxide scale can be determined.

2 Laser Flash Measurement

2.1 Laser Flash and Thermal Diffusivity

To measure the thermal diffusivity or rate of heat transfer within a material using the laser flash technique an unfocused laser beam that impinges onto the flat surface of a specimen is used. A thin layer close to the specimen surface absorbs the heat generated by the laser and the subsequent thermal distribution and heat flux within the material is then dependant only on the thermal diffusivity of the material. Thus by measuring the rate of heat transfer through the material the thermal diffusivity can be deduced. The temperature distribution through a homogeneous material may be described by the one-dimensional heat-conduction equation

$$\frac{\partial T}{\partial t} = \alpha \frac{\partial^2 T}{\partial^2 x} \ , \qquad (1)$$

where T is the temperature, t is the time, x is the thickness of the material and α is the thermal diffusivity. The thermal diffusivity can be calculated using

$$\lambda = \alpha \rho C \ , \qquad (2)$$

where λ is thermal conductivity, C is specific heat capacity at constant temperature and pressure and ρ is the density of the material. Thermal conductivity can be defined as the quantity of heat transmitted, due to unit temperature gradient, in unit time under steady conditions in a direction normal to a surface of unit area, when the heat transfer is dependent only on the temperature gradient. We can calculate the thermal conductivity for single layer homogeneous materials quite simply by using the laser flash data. To calculate the thermal conductivity for multi-layered systems a finite difference model has been developed which uses laser flash data. The laser flash analysis equipment (LFA) is schematically shown in Figure 1.

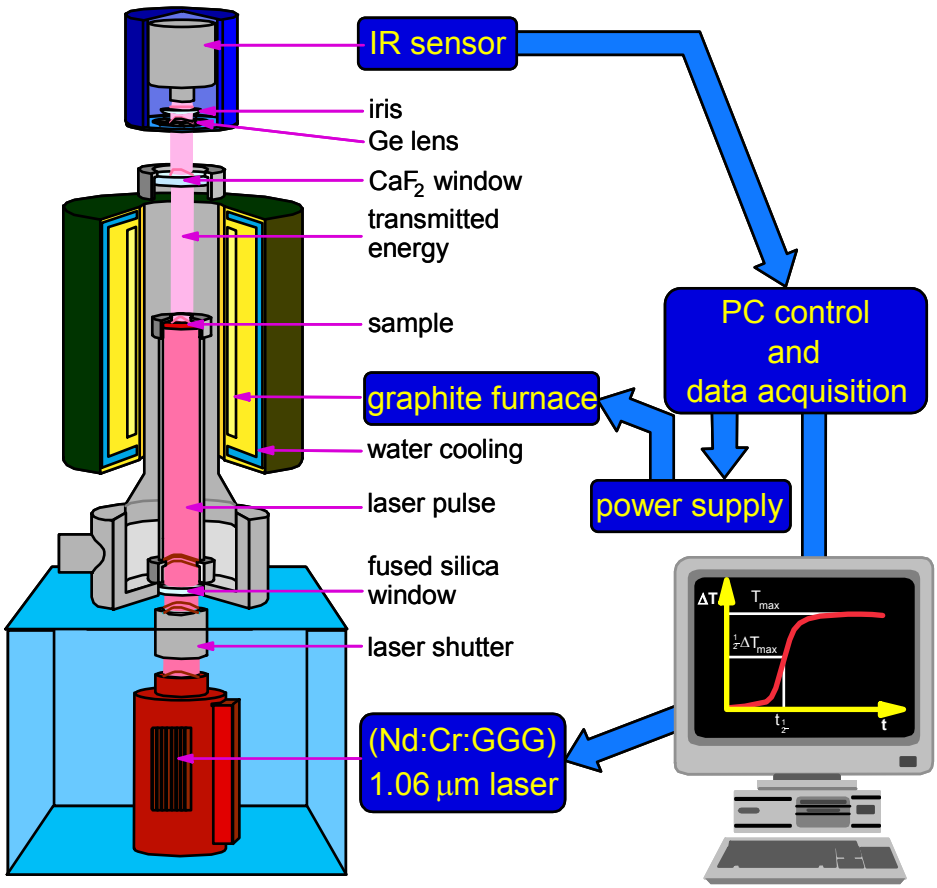

Figure 1 Schematic representation of the Laser Flash apparatus

2.2 Measurement Procedure

2.2.1 Principle

LFA thermal diffusivity measurement is made up of two basic steps, supplying an energy input on one side of the specimen and measuring the energy output and the time taken on the other side of the specimen. The initial energy input is supplied by heating the front face of a disc-shaped sample using a high intensity laser energy pulse or flash. The heat rise on the back face is monitored using an IR detector. From the temperature rise the thermal diffusivity can be calculated. These measurements can be performed over a range of temperatures by the use of a furnace, which is used to heat the sample to the desired temperature, as shown in Figure 1.

2.2.2 Specimen Preparation

For this work the test specimens were machined such that they had a diameter of 12.5 mm ± 0.05 mm, and a thickness between 1 and 3 mm. This was dependent on the amount of oxide scale grown. Ideally the thickness should not vary by more than 1% across the specimen. It has been estimated that a 1% error in the thickness will lead to an error of 2%

in the final diffusivity. The dimensions and composition of the P92 test specimens used for the examples in this report are presented in Table 1 and Table 2 respectively.

Table 1 Dimensions of P92 Laser Flash test specimens

Specimen ID	Flowing Steam Exposure		Diameter, mm	Thickness		
	Temperature, °C	Time, h		Total, mm	Metal, mm	Scale, μm
MEX46	-	-	12.46	1.753	1.753	0
MEX127	650	200	12.63	2.167	1.8659	150.7
MEX128	650	200	12.62	2.138	1.8584	139.6
MEX130	650	400	12.63	2.148	1.8671	140.7
MEX131	650	600	12.64	2.163	1.821	171.2
MEX133	650	800	12.67	2.166	1.844	161.2
MEX125	650	1000	12.69	2.302	1.802	207.3

Table 2 Composition of the P92 test specimens

Composition, weight %							
Fe	C	Cr	Mo	V	W	Nb	Ni
bal	0.12	8.85	0.42	0.2	1.85	0.07	0.042

2.2.3 Laser Flash Method

The pulse energy of the laser was set at a suitable value to produce a temperature rise of approximately 3 to 4 °C at the rear face of the sample. This is achieved by comparing the pulse width, which has an allowable range of 0.2 ms to 1.2 ms; to the time to reach half the value of the maximum temperature rise as shown in Figure 2. The operator aims to obtain a ratio of pulse width to half max time of 1:10 as a minimum but ideally 1:40.

Although a rise of around 4 °C is the minimum rise capable of giving a useful detector signal-to-noise ratio at ambient temperature, a low value is desirable both to reduce heat losses and to minimise the possibility of damage to the front face arising from the much larger temperature rise at that face.

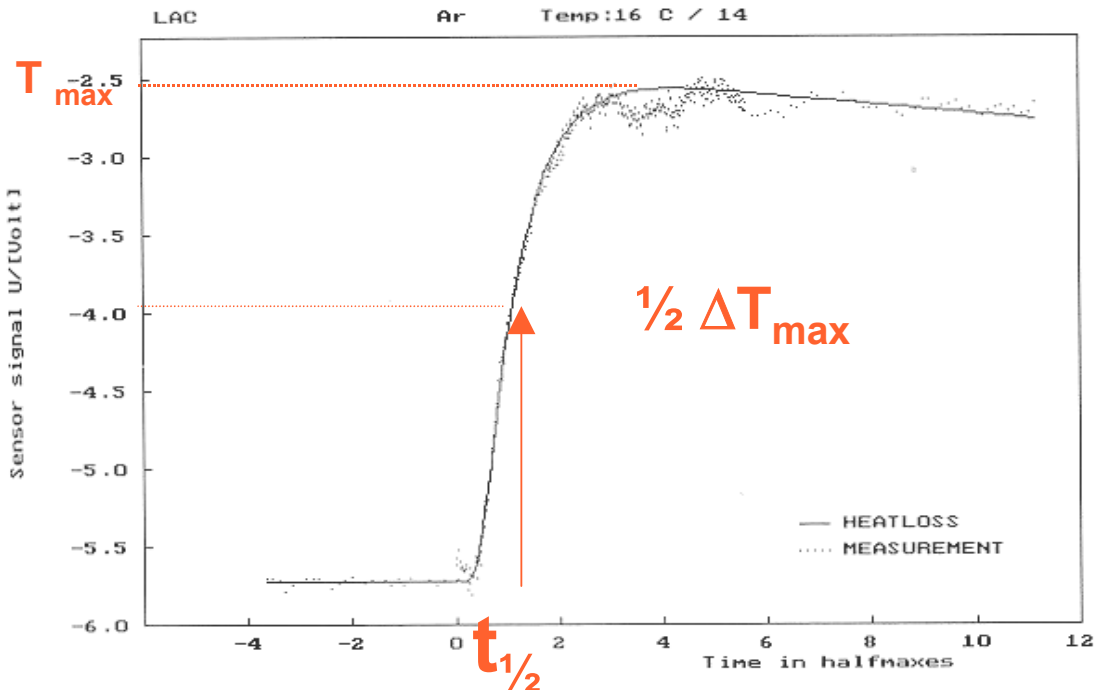

Figure 2 Heat rise in volts, detected from the rear face by the IR detector. Note the position of the half max time

The rear face temperature rise data provided by the infrared (IR) detector is automatically scaled and processed by the computer and the thermal diffusivity calculated using the user selected thermal diffusivity model.

The equipment used for this work presents the temperature rise as a voltage, which has been internally scaled by the operating software; ideally it would be better to obtain absolute temperature rise data without any uncontrollable amplification, but this is presently not possible.

2.2.4 Thermal Diffusivity Calculation

The relationship between the thermal diffusivity and the transient temperature rise can be derived by considering an idealised adiabatic model, and then applying corrections to allow for departures from this idealised situation.

The adiabatic model assumes that when the laser is fired, an instantaneous uniform pulse of energy is absorbed uniformly in a very thin surface layer of the sample. This energy then passes axially through the sample, and eventually raises the temperature of the rear surface. No heat is lost by the sample, and there is no radial heat flow. Under these conditions the thermal diffusivity α, is given by:

$$\alpha = 0.138785\frac{L^2}{t_{0.5}}, \qquad (3)$$

where L is the thickness of the sample, and $t_{0.5}$ is the time taken for the temperature of the rear face to reach half its maximum value [1]. Other rise times can be used.

Corrections are then made to the raw data to allow for errors introduced by the finite length of the laser pulse [2] or radiant heat losses [3,4]. The method used in this case is that of Dusza [5], which simultaneously corrects for both finite pulse and radial heat losses.

The adiabatic model also assumes a one-dimensional heat flow and that there is no heat loss from the test piece. To maintain these boundary conditions radial heat flow is minimised by reducing the area of contact between the sample and its support, and by ensuring that the ratio of the flat area of the disc to the curved area is large (i.e., that the sample is thin).

2.2.5 Error Analysis

2.2.5.1 Sources of Error

The sources of error in the LFA can be attributed to the following:

- Sample thickness
- Calculation of a time constant ($t_{0.5}$)
- Computer / data grabber time base (τ)
- Temperature measurement
- Others: non-uniformity of laser; baseline drift; radial heat losses

These errors contribute to the measurement uncertainty as detailed below.

2.2.5.2 Sample Thickness

Specimens are measured with a micrometer giving a typical measurement uncertainty of ± 0.003 mm. Variation in the thickness of up to 1%, or ± 0.02 mm for a 2 mm thick specimen is allowed. Accordingly, any uncertainty in the measurement of thickness is very much less than the variation in the specimen thickness, and can be ignored. As the square of the thickness is used, the maximum allowed uncertainty in the thickness, L, for a 2 mm thick specimen is ± 0.04 mm² in 4 mm², or 1.0%.

2.2.5.3 Time Constant ($t_{0.5}$) and Computer / Data grabber Time base (τ)

The computer / data grabber time base error is much less than the overall error in calculating $t_{0.5}$, and can be ignored. As it is difficult to directly calculate the error associated with $t_{0.5}$, it is subsumed in the Repeatability statement, given below.

2.2.5.4 Temperature Measurement

The corrected sample temperature has an uncertainty of ± 5 °C from RT to 1000 °C and ± 7 °C from 1000 °C to 1650 °C. The effect of any temperature error on the measured thermal diffusivity will be sample material dependent and is difficult to evaluate. It will depend on how rapidly the thermal diffusivity of the material changes with changing temperature. Instead of evaluating this error directly it is subsumed in the Repeatability statement below. However, it is also stated separately, see the Repeatability statement below.

2.2.5.5 Other Errors

There are various other sources of uncertainty: non-uniformity of the laser, baseline drift, radial heat losses, etc. These are all subsumed in the Repeatability statement below.

2.2.6 Repeatability of the measurement

Measurements have been made on a sample of ASS Steel (SRM 1461) between 13/11/97 and 29/10/98, and also on a number of ASX Graphite samples between 6/10/97 and 7/10/98. Figure 3 shows the distributions of the measured data for each material around a mean value.

From Figure 3, it can be seen that the data follows a normal distribution curve. Taking the worst case (the ASX graphite), 95% of the data falls within 2.4% of the best-fit line. Therefore the overall Repeatability of ±2.4% can be assumed to be indicative of the Laser Flash technique. Of this 2.4% value, it has been estimated that 1% is due to errors in the temperature measurement (equivalent to ±5°C at 800°C for graphite), which is listed separately in the summary table below. This leaves the Repeatability uncertainty as 1.4%.

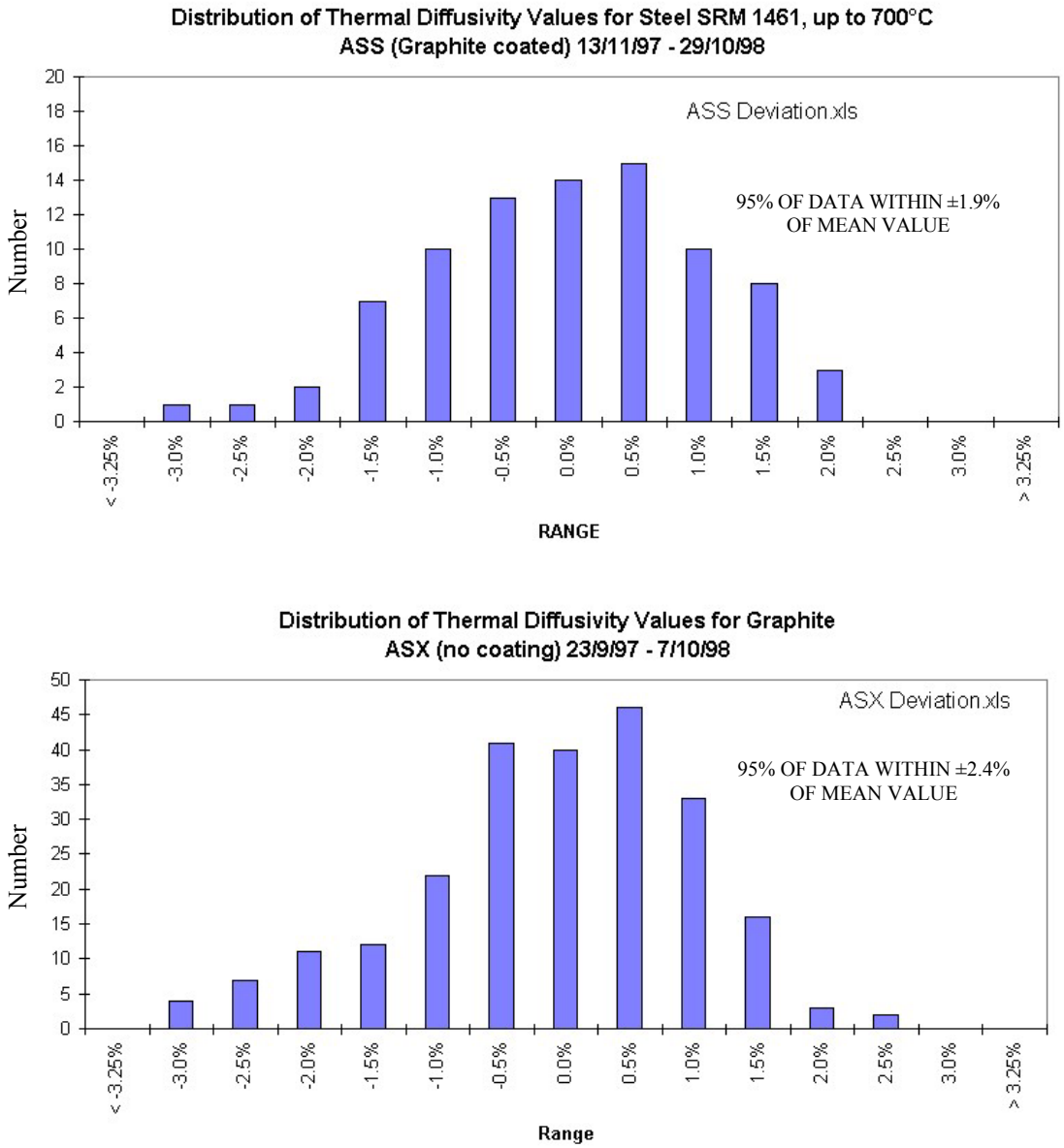

Figure 3 Distribution of thermal diffusivity values for two materials, illustrating the repeatability of the Laser Flash technique.

2.2.7 Overall Uncertainty

The reproducibility of the apparatus is better than 2%, but for routine test work an uncertainty of 4% within the 95% confidence level and coverage factor of 2 is quoted. The sources of uncertainty, within the 95% confidence limit, associated with measurements in the apparatus are presented in Table 3:

Table 3 Sources and contribution to the uncertainty of thermal diffusivity measurements using the Laser Flash technique.

Source of Uncertainty	Value ±	Probability Distribution	Divisor	u_i ± units
Repeatability	1.4	Normal	1	1.4
Square of specimen thickness	1.0	Rectangular	√3	0.6
Furnace temperature	1.0	Normal	1	1.0
Combined standard uncertainty	-	Normal	-	2
Expanded uncertainty	-	Normal (k=2)	-	4

Further details on uncertainty evaluation can be found in the "Guide to the expression of uncertainty in measurement" [6].

3 Thermal Diffusivity Measurements of P92

3.1 Thermal Diffusivity of as-received P92

Laser Flash thermal diffusivity measurements have been conducted on as-received un-oxidised samples of P92, dimensions and composition shown in Tables 1 and 2. Measurements were conducted in argon over a temperature range of 13 °C to 718 °C. Prior to the measurement the test piece was sand blasted and it's dimensions measured and recorded. The test piece was found to have a diameter of 12.46 mm and a thickness of 1.732 mm. Figure 4 shows the thermal diffusivity values for the as received P92 material as a function of temperature.

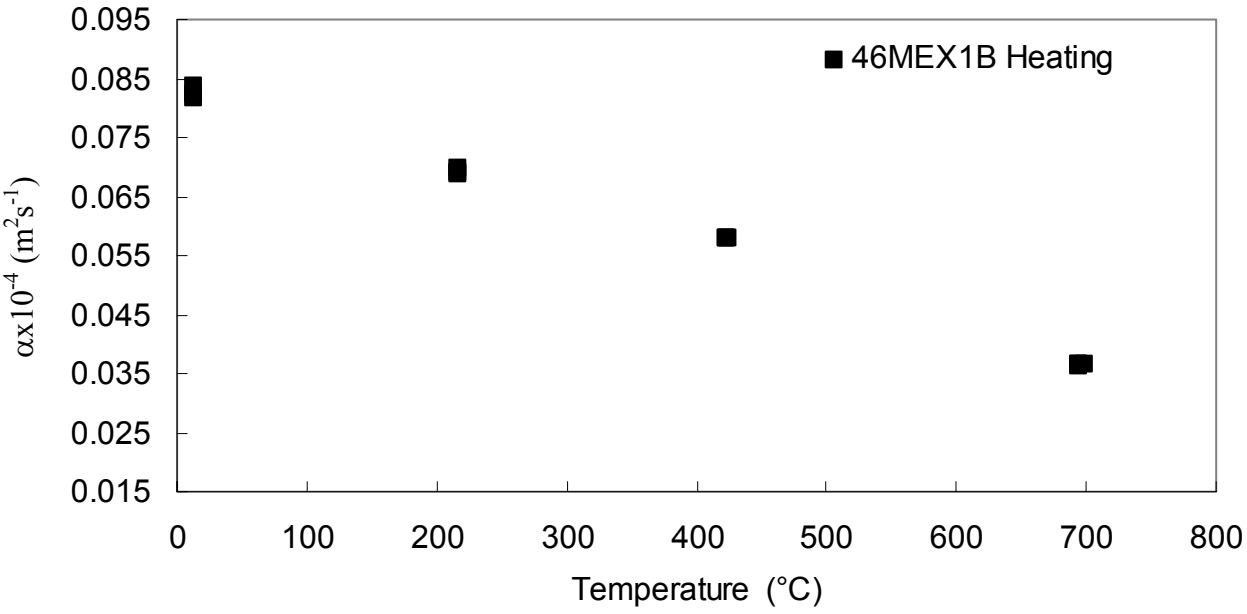

Figure 4 Thermal diffusivity of the as-received P92, measured using the Laser Flash technique

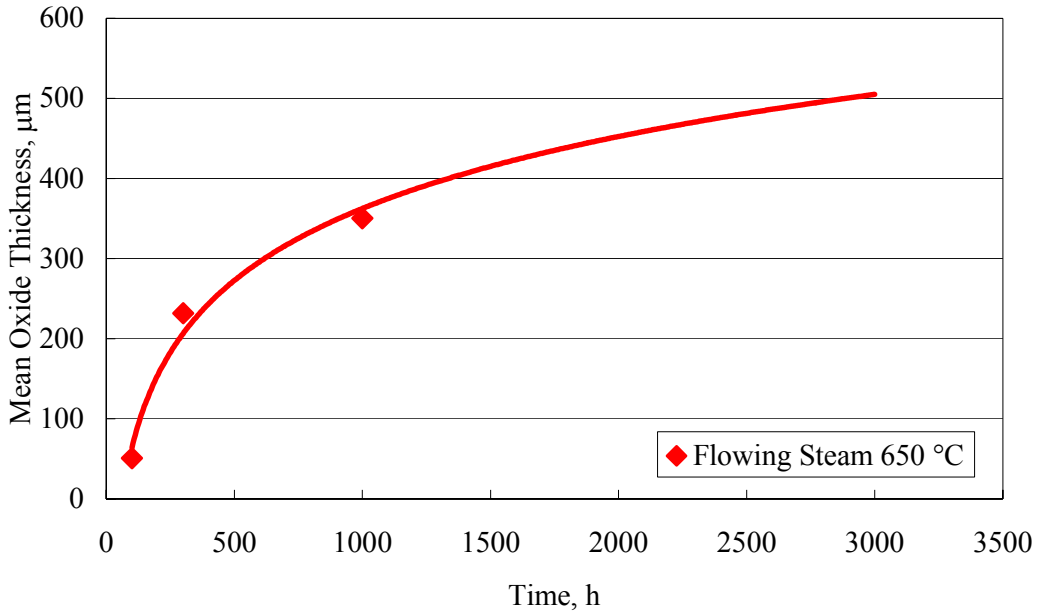

Figure 5 Mean oxide thickness with exposure time for flowing steam at 650 °C

3.2 Thermal Diffusivity of oxidised P92

P92 test pieces were machined and oxidised in flowing steam at 650 °C for between 200 and 1000 hours, with the intention of producing a series of scale thickness up to 350 µm (Figure 5). However the measured scale thickness of the LFA specimens were lower than the expected values, although still with the expected variation in scale thickness.

3.3 Thermal Diffusivity of Copper/Braze

As a check for the TherMOL model, LFA measurements were also performed on copper, braze and a two layered sample of copper and braze. Performing the measurements on these well-characterised materials provided data that could be used to validate the TherMOL model. For these purposes LFA measurements were performed over a range of temperatures.

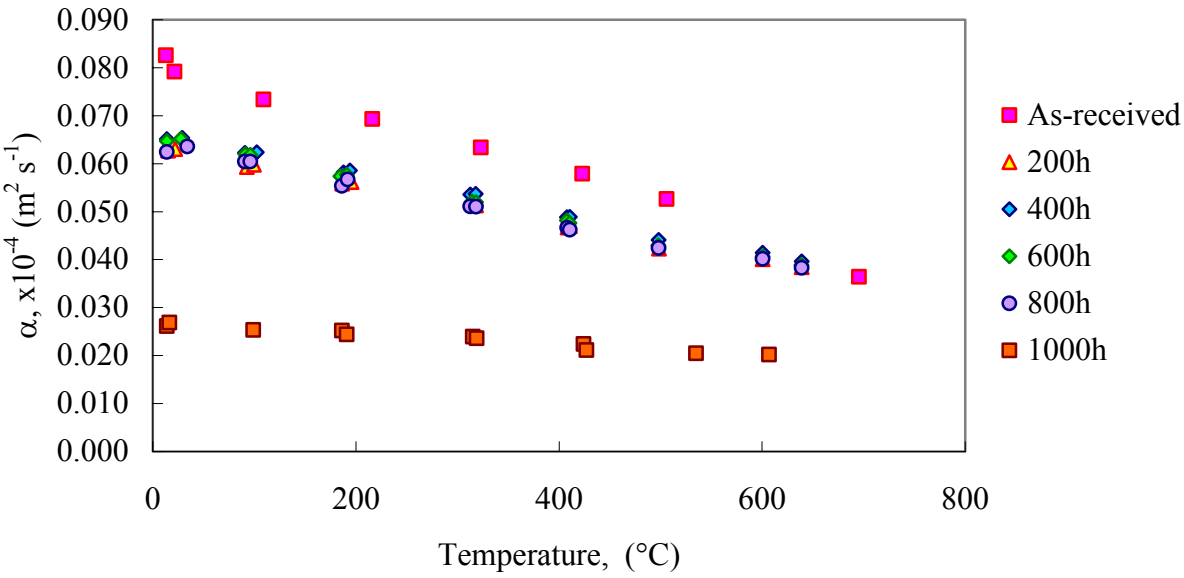

Figure 6 Thermal Diffusivity values for P92 oxidised in flowing steam for 200h, illustrating the effect that spallation has on thermal diffusivity

The Thermal Diffusivity results are shown in Figure 6, which clearly shows that the presence of an oxide scale reduces the thermal diffusivity of the test specimen. The thermal diffusivity values of the test piece that had been oxidised in flowing steam at 650 °C for 1000 h are much lower than would be expected from the other results. Also of interest is the fact that the value remains relatively constant over the 600 °C temperature range. This behaviour is caused by spallation of the oxide scale away from the substrate. This was also observed in samples oxidised for 200 h, although these results have not been included in Figure 6. On repeating the test for the 200 h exposure time, thermal diffusivities, which agree with the other samples, were recorded, and are presented in Figures 6. It is also interesting to note that the actual thickness of the oxide scale does not have a great effect on the thermal diffusivity, but that the very presence of the scale and/or the substrate-scale interface seems to be the more dominant factor in affecting the thermal diffusivity. However, it should be noted that the oxide thickness did not vary to the extent that was anticipated from Figure 5.

4. Thermal Conductivity

4.1 Two-dimensional Heat-conduction Model

The NPL developed software tool TherMOL was used to calculate the temperature profiles through the specimens during the laser flash analysis. Multi-parameter optimisation routines based on the Nelder Mead Algorithm [7, 8] were used to determine conductivity and heat flux values to fit the model to the experimental data.

In this section the basic theory used by TherMOL to determine the two-dimensional temperature profile for a multi-layered system is described. TherMOL uses an explicit finite difference method, where simple energy balances are constructed around areas surrounding each node on the mesh, to calculate the temperature for a set time step. Constant heat flux boundary conditions at discrete time steps are used to simulate the laser flash heating of the specimen.

4.1.1 Geometry

Consider a layered system consisting of N layers of homogeneous materials with total thickness L and width W as shown in Figure 7.

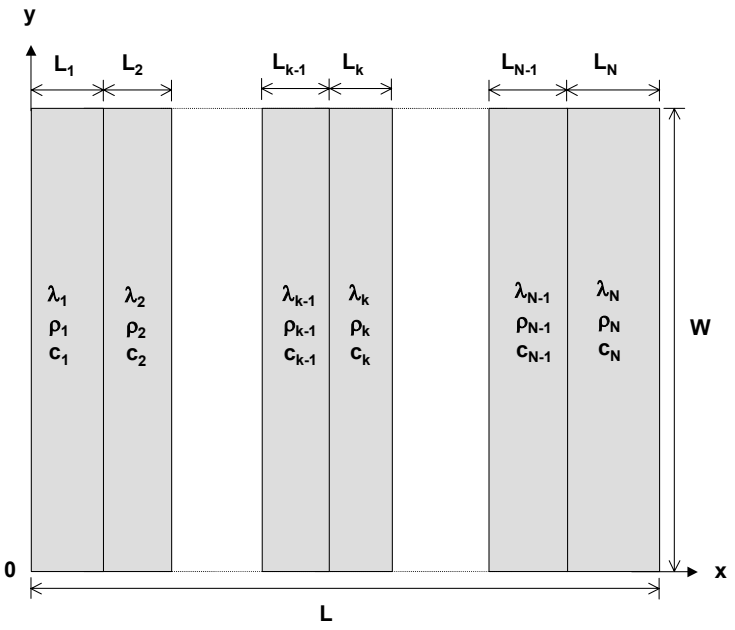

Figure 7 Diagram showing the geometry, dimensions and the associated coordinate system for a multi-layered system consisting of N homogeneous materials

A two-dimensional x-y coordinate system (shown in Figure 7) is used to represent the layered system where the thickness direction of the layered system is represented by the

x-coordinate and the width direction of the layered system is represented by the y-coordinate. In Figure 7 the thickness, thermal conductivity, density and specific heat capacity of the k^{th} layer (where k = 1…N) are given by L_k, λ_k, ρ_k and c_k respectively.

In order to calculate the temperature distribution numerically it is necessary to describe the material sample using a discrete mesh as shown in Figure 8. The two-dimensional x-y mesh consists of n_x nodes in the x-direction ($0…n_x$) and n_y nodes in the y-direction ($0…n_y$), which are equally spaced at a distances Δx and Δy apart respectively. The grid dimensions are set up so that $L = n_x \times \Delta x$ and $W = n_y \times \Delta y$. The four boundaries x = 0, x = L, y = 0 and y = W will be referred to by the numbers 1, 2, 3 and 4 respectively and parameters associated with the four boundaries will be referred to by the appropriate superscripts or subscripts 1, 2, 3 and 4.

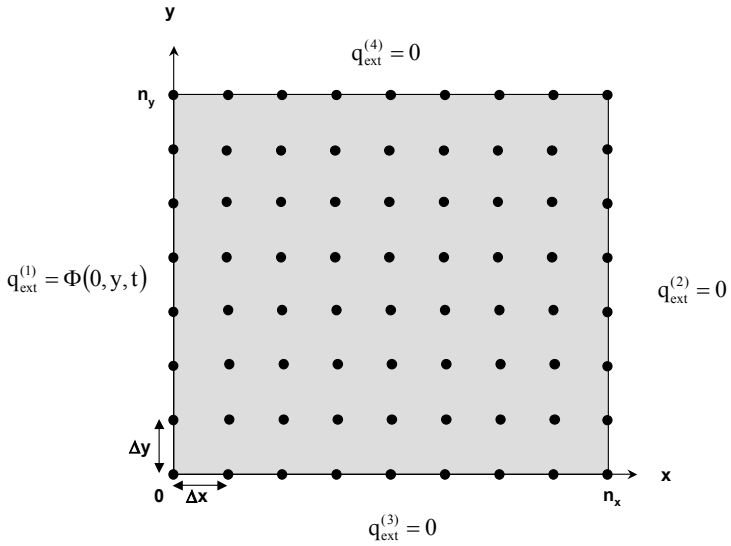

Figure 8 Diagram showing the node structure, mesh dimensions and applied boundary conditions for the TherMOL model

4.1.2 Initial and Boundary Conditions

Let $T_{m,n}^{p}$ be the temperature of the $(m,n)^{th}$ node at the p^{th} time step such that $(x,y,t) = (m.\Delta x, n.\Delta y, p.\Delta t)$, where Δt is a fixed discrete time interval and the total number time steps are n_t such that $p = 0…n_t$. Initially at t = 0 all nodes are assumed to have the value of the steady state temperature surrounding the material, such that $T_{m,n}^{0} = T_{ext}$ for all m and n. TherMOL can be used to model the heat transfer through the layered material when subjected to various heat flux boundary conditions. In Figure 8, the normal component of the heat flux vector at the surface i (where i = 1..4) is defined as $q_{ext}^{(i)}$. It was assumed that for the duration of the simulation there was very little heat transfer at the boundaries apart from the laser flash, and radiation effects were negligible. To simulate these boundary conditions the model used a zero flux boundary condition for boundaries 2, 3 and 4 and the layered system was subjected to the time dependent heat flux function Φ at boundary 1 (x = 0), such that

$$q_{ext}^{(1)} = \Phi(y,t) \ . \qquad (4)$$

The heat flux input in (4) simulates the laser pulse and has a value $\Phi(y,t)$ that is dependent on the position along boundary 1 and time.

4.1.3 Finite Difference Equations

The model uses an explicit solution method where the temperature at each node is written as a function of the temperatures of the nodes at the end of the previous time step. The equation at a node is derived by considering the heat flow into and out of a small element surrounding the node and stating that any net heat flow into or out of the element raises or lowers the temperature of that element accordingly.

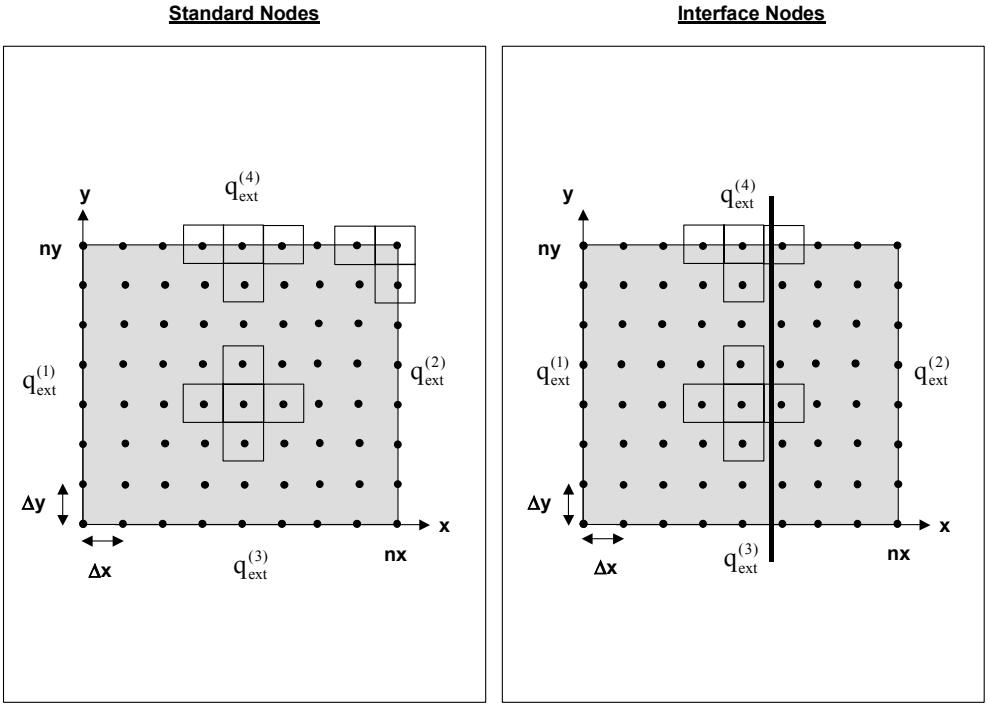

Figure 9 Diagram showing the placement of internal, side, corner and interface nodes with the appropriate boundary conditions on a two-dimensional grid

In solving the heat transfer in a block of material using finite differences there are five different energy balances that must be constructed and solved. Each different energy balance is associated with a different node type, which are: internal, side, internal interface, corner internal interface and side interface nodes as shown in Figures 9 and 10.

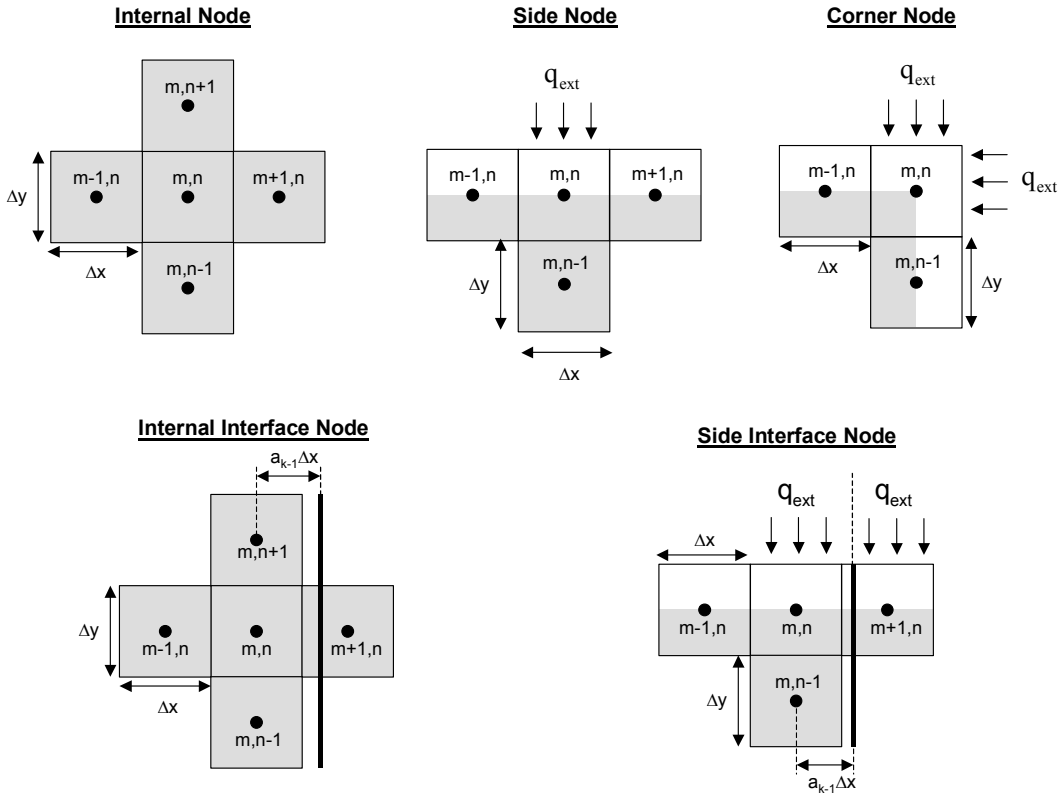

Figure 10 Diagrams showing the relevant nodes used in the derivation of two-dimensional finite difference equations for internal, side and corner nodes

Heat transfer through the specimen is assumed to be driven by conduction where for a constant volume of material away from any boundaries the heat fluxes from x to x_1 and y to y_1 are given by $q_{x\to x_1}$ and $q_{y\to y_1}$ respectively, and may be defined using Fourier's Law [9] such that

$$q_{x\to x_1} = -\lambda \frac{\partial T}{\partial x}, \qquad q_{y\to y_1} = -\lambda \frac{\partial T}{\partial y}, \tag{5}$$

where the proportionality constant λ is the thermal conductivity. It is assumed for consistency that in all finite difference equation derivations the heat flow from all directions is ***into*** the node (m, n). Using a similar approach outlined in Incropera and DeWitt [10] the law of conservation of energy can be applied, to account for the heat flow in two orthogonal directions (x and y), to give

$$\rho C \frac{\partial T}{\partial t}\frac{\Delta y}{2}\Delta x = q^{p}_{(m,n-1)\to(m,n)}\Delta x + q^{p}_{(m,n+1)\to(m,n)}\Delta x + q^{p}_{(m+1,n)\to(m,n)}\Delta y + q^{p}_{(m-1,n)\to(m,n)}\Delta y, \tag{6}$$

$$(m = 1\ldots n_x\text{-}1,\ n = 1\ldots n_y\text{-}1,\ p = 0\ldots n_t\text{-}1),$$

where the temperature change with time is given by $\partial T/dt$. To solve the temperature distribution numerically the appropriate conservation equation must be used for each *internal node* of unknown temperature. Using (5) and (6)

$$T_{m,n}^{p+1} = \alpha r_x \left(T_{m+1,n}^{p} + T_{m-1,n}^{p}\right) + \alpha r_y \left(T_{m,n+1}^{p} + T_{m,n-1}^{p}\right) + \left(1 - 2\alpha r_x - 2\alpha r_y\right) T_{m,n}^{p} \quad , \qquad (7)$$

$$(\text{for } m = 1\ldots n_x\text{-}1,\ n = 1\ldots n_y\text{-}1,\ p = 0\ldots n_t\text{-}1) \ ,$$

where α is given by equation (2) and the parameters r_x and r_y in (7) are defined as

$$r_x = \frac{\Delta t}{\Delta x^2} \ , \qquad r_y = \frac{\Delta t}{\Delta y^2} \ . \qquad (8)$$

If we now consider that boundary 1 is subjected to discrete heat flux Φ_n^{p+1} at a time p+1 and for boundaries 2 to 4 the heat fluxes are zero such that $q_{ext}^{(2)} = q_{ext}^{(3)} = q_{ext}^{(4)} = 0$, then forming similar balances as (6) and solving for the $(m, n)^{th}$ node on the boundary the *side nodes* for boundaries 1 to 4 are given by

$$T_{m,n}^{p+1} = 2\alpha r_x T_{m+1,n}^{p} + \alpha r_y \left(T_{m,n+1}^{p} + T_{m,n-1}^{p}\right) + \left(1 - 2\alpha r_x - 2\alpha r_y\right) T_{m,n}^{p} + \frac{2}{\rho C}\frac{\Delta t}{\Delta x}\Phi_n^{p+1} \ , \qquad (9)$$

$$(\text{for } m = 0,\ n = 1\ldots n_y\text{-}1,\ p = 0\ldots n_t\text{-}1) \ ,$$

$$T_{m,n}^{p+1} = 2\alpha r_x T_{m-1,n}^{p} + \alpha r_y \left(T_{m,n+1}^{p} + T_{m,n-1}^{p}\right) + \left(1 - 2\alpha r_x - 2\alpha r_y\right) T_{m,n}^{p} \quad , \qquad (10)$$

$$(\text{for } m = n_x,\ n = 1\ldots n_y\text{-}1,\ p = 0\ldots n_t\text{-}1) \ ,$$

$$T_{m,n}^{p+1} = 2\alpha r_y T_{m,n+1}^{p} + \alpha r_x \left(T_{m+1,n}^{p} + T_{m-1,n}^{p}\right) + \left(1 - 2\alpha r_x - 2\alpha r_y\right) T_{m,n}^{p} \quad , \qquad (11)$$

$$(\text{for } m = n_x\text{-}1,\ n = 0,\ p = 0\ldots n_t\text{-}1) \ ,$$

$$T_{m,n}^{p+1} = 2\alpha r_y T_{m,n-1}^{p} + \alpha r_x \left(T_{m+1,n}^{p} + T_{m-1,n}^{p}\right) + \left(1 - 2\alpha r_x - 2\alpha r_y\right) T_{m,n}^{p} \quad , \qquad (12)$$

$$(\text{for } m = 1\ldots n_x\text{-}1,\ n = n_y,\ p = 0\ldots n_t\text{-}1) \ .$$

Forming similar balances as in (8) and solving for the $(m, n)^{th}$ node at the corners of the boundaries, yields the following finite difference equations for the *corner nodes*

$$T_{0,0}^{p+1} = 2\alpha\left(r_x T_{1,0}^{p} + r_y T_{0,1}^{p}\right) + \left(1 - 2\alpha r_x - 2\alpha r_y\right) T_{0,0}^{p} + \frac{2}{\rho C}\frac{\Delta t}{\Delta x}\Phi_0^{p+1} \ , \qquad (13)$$

$$T_{0,ny}^{p+1} = 2\alpha\left(r_x T_{1,ny}^{p} + r_y T_{0,ny-1}^{p}\right) + \left(1 - 2\alpha r_x - 2\alpha r_y\right) T_{0,ny}^{p} + \frac{2}{\rho C}\frac{\Delta t}{\Delta x}\Phi_{ny}^{p+1} \ , \qquad (14)$$

$$T_{nx,0}^{p+1} = 2\alpha\left(r_y T_{nx,1}^{p} + r_x T_{nx-1,0}^{p}\right) + \left(1 - 2\alpha r_x - 2\alpha r_y\right) T_{nx,0}^{p} \quad , \qquad (15)$$

$$T_{nx,ny}^{p+1} = 2\alpha\left(r_y T_{nx,ny-1}^{p} + r_x T_{nx-1,ny}^{p}\right) + \left(1 - 2\alpha r_x - 2\alpha r_y\right) T_{nx,ny}^{p} \quad , \tag{16}$$

where in (13-16) p = 0...n_t-1. If we now consider a layered system where the layers are homogenous materials through which heat may be transferred. In such a system the k^{th} layer contains n_x^k nodes in the x-direction and n_y+1 nodes in the y-direction. There are two more node types for which energy balances must be derived; internal interface nodes and side interface nodes. The finite difference equations for a single homogeneous block of material derived for internal nodes, side nodes and corner nodes apply for a layered system as long as the nodes do not lie adjacent to an interface. For the *internal nodes* that lie to the *left of an interface*, as shown in Figure 10, the following finite difference equation should apply

$$\begin{aligned} T_{m,n}^{p+1} = {} & \frac{1}{\rho_{k-1} C_{k-1}} \left[\lambda_{k-1} r_x T_{m-1,n}^{p} + \frac{\Delta t}{\Delta x} \frac{T_{m+1,n}^{p}}{R_{k-1}^{tot}} + \lambda_{k-1} r_y \left(T_{m,n-1}^{p} + T_{m,n+1}^{p} \right) \right] \\ & + \left[1 - \frac{1}{\rho_{k-1} C_{k-1}} \left\{ \lambda_{k-1} r_x + \frac{\Delta t}{\Delta x} \frac{1}{R_{k-1}^{tot}} + 2 r_y \lambda_{k-1} \right\} \right] T_{m,n}^{p} , \end{aligned} \tag{17}$$

$$(\text{for } m = (k\text{-}1)\, n_x^k ,\ n = 1 \ldots n_y\text{-}1,\ k = 1 \ldots N,\ N \geq 2) ,$$

and for *internal nodes* that lie to the *right of an interface*

$$\begin{aligned} T_{m,n}^{p+1} = {} & \frac{1}{P_{k-1}} \left[\lambda_k r_x T_{m+1,n}^{p} + \frac{\Delta t}{\Delta x} \frac{T_{m-1,n}^{p}}{R_{k-1}^{tot}} + r_y \left(\chi_{k-1}^{l} \lambda_{k-1} + \chi_{k-1}^{r} \lambda_k \right) \left(T_{m,n-1}^{p} + T_{m,n+1}^{p} \right) \right] \\ & + \left[1 - \frac{1}{P_{k-1}} \left\{ \lambda_k r_x + \frac{\Delta t}{\Delta x} \frac{1}{R_{k-1}^{tot}} + 2 r_y \left(\chi_{k-1}^{l} \lambda_{k-1} + \chi_{k-1}^{r} \lambda_k \right) \right\} \right] T_{m,n}^{p} , \end{aligned} \tag{18}$$

$$(\text{for } m = 1 + (k\text{-}1)\, n_x^k ,\ n = 1 \ldots n_y\text{-}1,\ k = 2 \ldots N,\ N \geq 2) ,$$

where R_{k-1}^{tot} is the total thermal resistance between the nodes on either side of the interface and is given by

$$R_{k-1}^{tot} = \frac{a_{k-1} \Delta x}{\lambda_{k-1}} + \frac{\left(1 - a_{k-1}\right) \Delta x}{\lambda_k}, \qquad (\text{for } k = 2 \ldots N) , \tag{19}$$

In (19) $a_{k-1}\Delta x$ is the x-displacement between the node on the left of the interface and the actual interface (see Figure 10). It is assumed that $a_{k-1} \geq 1/2$ for all the finite difference equations derived for layered systems in this section, however it should be noted that similar derivations can be made for $a_{k-1} < 1/2$, which are not included in this report. It is convenient to define the displacement ratios χ_{k-1}^{l} and χ_{k-1}^{r} for the node on the right of the boundary in (17-18) are defined as

$$\chi^{l}_{k-1} = \left(a_{k-1} - \frac{1}{2} \right), \qquad \chi^{r}_{k-1} = \left(\frac{3}{2} - a_{k-1} \right) , \tag{20}$$

The corresponding ratio function P_{k-1} for the k-1th interface, of the densities (ρ_{k-1} and ρ_k) and specific heats (C_{k-1} and C_k) is

$$P_{k-1} = \chi^{l}_{k-1}\rho_{k-1}c_{k-1} + \chi^{r}_{k-1}\rho_k c_k \ . \tag{21}$$

The finite difference equations for the *side nodes* that lie to the *left of an interface* on boundary 4 are

$$\begin{aligned} T^{p+1}_{m,n} = {} & \frac{1}{P_{k-1}} \left[\lambda_{k-1} r_x T^{p}_{m-1,n} + \frac{\Delta t}{\Delta x} \frac{T^{p}_{m+1,n}}{R^{tot}_{k-1}} + 2\lambda_{k-1} r_y T^{p}_{m,n-1} \right] \\ & + \left\{ 1 - \frac{1}{P_{k-1}} \left(\lambda_{k-1} r_x + \frac{\Delta t}{\Delta x} \frac{1}{R^{tot}_{k-1}} + 2\lambda_{k-1} r_y \right) \right\} T^{p}_{m,n} . \end{aligned} \tag{22}$$

(for, m = (k-1) n^{k}_{x} , n = 1…n_y-1, k = 2…N, N ≥ 2)

and for the *side nodes* that lie to the *right of an interface* on boundary 4

$$\begin{aligned} T^{p+1}_{m,n} = {} & \frac{1}{P_{k-1}} \left[\lambda_k r_x T^{p}_{m+1,n} + \frac{\Delta t}{\Delta x} \frac{T^{p}_{m-1,n}}{R^{tot}_{k-1}} + 2r_y \left[\chi^{l}_{k-1}\lambda_{k-1} + \chi^{r}_{k-1}\lambda_k \right] T^{p}_{m,n-1} \right] \\ & + \left\{ 1 - \frac{1}{P_{k-1}} \left(\lambda_k r_x + \frac{\Delta t}{\Delta x} \frac{1}{R^{tot}_{k-1}} + 2r_y \left[\chi^{l}_{k-1}\lambda_{k-1} + \chi^{r}_{k-1}\lambda_k \right] \right) \right\} T^{p}_{m,n} . \end{aligned} \tag{23}$$

(for m = 1+(k-1) n^{k}_{x} , n = 1…n_y-1, k = 2…N, N ≥ 2)

where the displacement ratios χ^{l}_{k-1} and χ^{r}_{k-1} are given by (20) and the ratio function P_{k-1} is given by (21). Similar expressions to (22) and (23) may be derived for boundary 3. In (17-18) and (22-23) λ_{k-1} and λ_k are the thermal conductivities for the k-1th and kth layers respectively. It should also be noted that the associated thermal diffusivities of the k-1th and kth layers are α_{k-1} and α_k respectively, which may be calculated by

$$\alpha_{k-1} = \frac{\lambda_{k-1}}{\rho_{k-1}c_{k-1}} , \qquad \alpha_k = \frac{\lambda_k}{\rho_k c_k} \ . \tag{25}$$

The finite difference equations (7), (9-12), (13-16), (17-18) and (22-23) may be used to determine the temperature of a multi-layered system at the time step p+1. It should be noted that for linear analyses (no radiation), a simpler method for calculating temperatures in multi-layered systems has now been adopted. This follows an approach outlined by Duncan, Urquhart and Roberts [11] for multi-material mass diffusion systems, where the balance of mass fluxes is analogous to the balance or thermal fluxes. All the nodes lie on a variable mesh and are assumed not to lie on any interfaces or boundaries, hence there is no need to derive separate equations for interface or boundary nodes.

4.2 Model Validation

To validate the TherMOL model three samples were produced from well-characterised materials, these consisted of a sample of pure copper, a sample cast from a brazing rod and a composite sample of copper and braze (essentially a two layer system). Laser flash measurements were made on each sample over a range of temperatures. The data from the laser flash were exported and formatted for the TherMOL model. The model requires the following information:

- Heat Flux
- Initial temperature
- Temperature rise with time data
- Density
- Specific heat capacity
- Area of the sample face
- Sample thickness

The heat flux of the laser flash was estimated from the voltage setting of the pulse. From this voltage and the knowledge that the laser has a reported resistance of 1 Ω, the maximum possible heat flux can be calculated. In practice the heat flux impinging on the sample is much lower than this maximum value due to energy losses caused by imperfections in the laser, heat loss etc. For this reason the initial step in fitting the experimental data is to adjust the magnitude of the heat flux used in the model calculations such that the heat rise on the far face is at the same level as the experimental data. This adjustment of the heat flux has been shown to have little effect on the final thermal conductivity value calculated by the model, but does effect the final temperature of the far face.

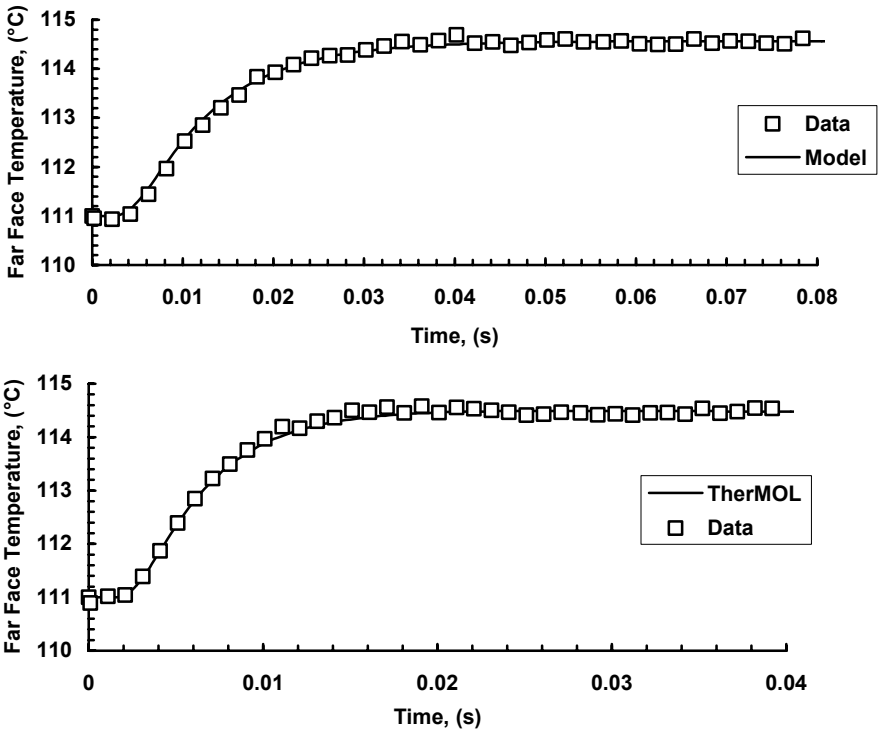

Figure 12 Laser flash data and the TherMOL fit for (a) copper with a heat flux of 6.52x10^7 Wm^{-2} for 0.0004 s, and (b) copper and braze sample with a heat flux of 4.10x10^7 Wm^{-2} for 0.0006 s.

With regards to the temperature rise with time data it is important that this is a true measure of the temperature, and not a scaled voltage. After exporting the data from the laser flash equipment it was necessary to convert the raw voltage values from the IR sensor to temperature values, which the model requires. For the equipment at NPL a 1V increase in the IR sensor is equivalent to a 1 °C increase in temperature. This data was then adjusted, to account for the internal amplification applied to the raw readings, such that the temperature rise matched that reported by the laser flash software.

Once the data had been formatted in this manner it could be used in the TherMOL software, an example of which is shown in Figure 12. This figure shows the TherMOL fit to the experimental laser flash data for the copper sample and the copper/braze sample. The properties of the copper and the copper/braze layers are presented in Table 4. If we compare the calculated thermal conductivity values of the materials to published data book values, then it is clear that the TherMOL model gives a very good prediction, within the limits of experimental errors.

Table 4 Properties of the layers used to validate the TherMOL model.

Sample	Layer	Layer Thickness (mm)	Sample Diameter (mm)	Thermal Conductivity ($Wm^{-1}K^{-1}$)	Density (kgm^{-3})	Specific Heat Capacity, ($Jkg^{-1}K^{-1}$)	Thermal Conductivity from literature ($Wm^{-1}K^{-1}$)
Copper	Copper	2.094	12	362	8930	397	385
Copper/Braze	Copper	1.015	12	362	8930	397	385
	Braze	1.015	12	118	8700	377	116

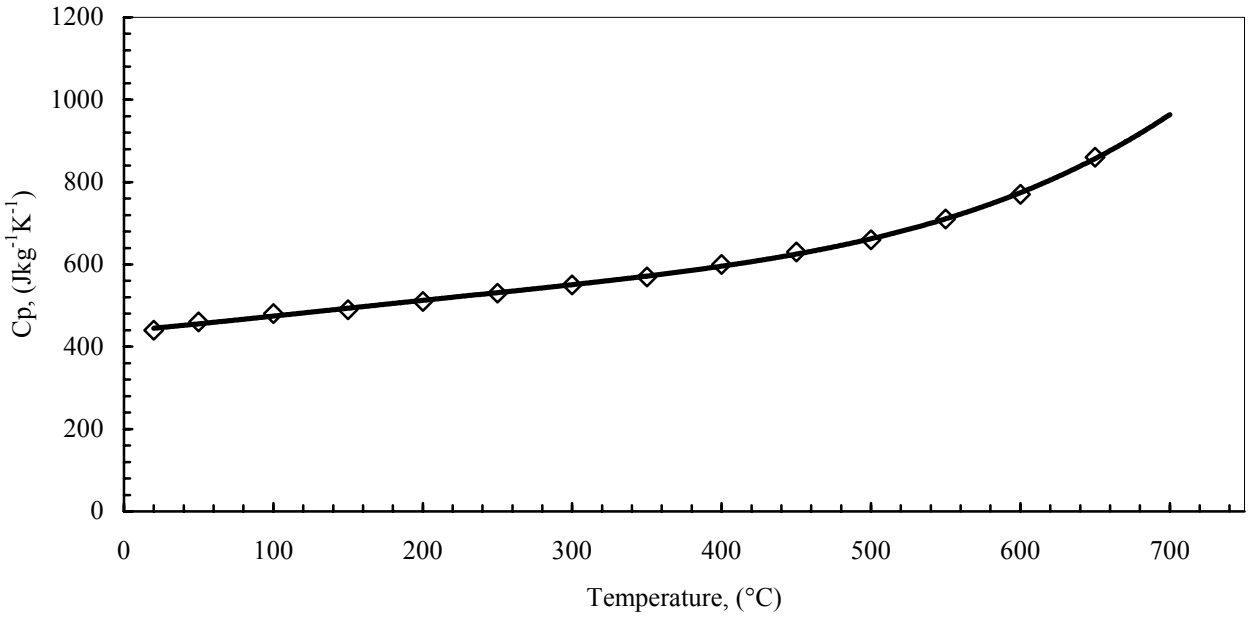

Figure 13 A polynomial fit of Cp versus temperature

4.2.2 Model Calculations for P92

To be able to fully analyse the oxide scale grown on the P92 sample as described in section 3, it is first necessary to establish the thermal properties of the P92 substrate. Data from the laser flash measurements on un-oxidised P92 was used to establish the thermal conductivity of the P92 substrate over a range of temperatures. This was achieved in the following manner.

Laser flash measurements were conducted from room temperature up to around 700 °C. The thermal diffusivity values calculated by the laser flash equipment were then used in conjunction with calculated specific heat values, interpolated from published specific heat capacity values for P91 [12], as shown in Figure 13.

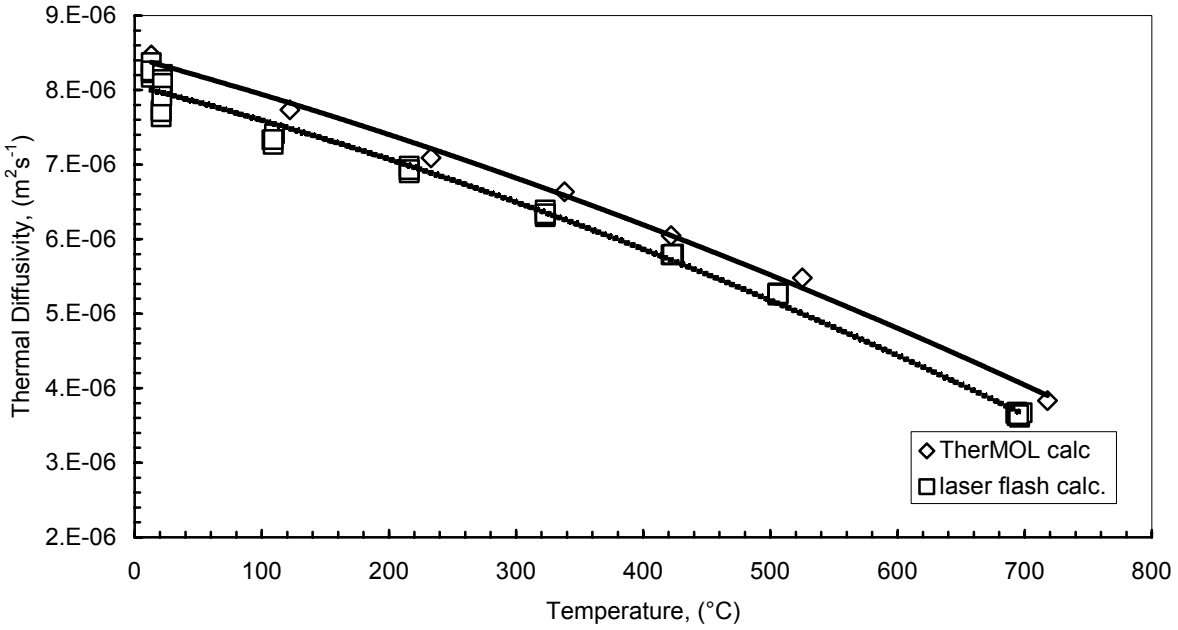

Figure 14 Comparison of the thermal diffusivity calculated by the laser flash equipment and the TherMOL model for unoxidised P92

The temperature rise with time data obtained from the laser flash was then used to calculate the thermal diffusivity as defined in (1), using the TherMOL model. The values obtained are compared with the values calculated by the laser flash equipment in Figure 14. It should be noted that the TherMOL model uses the whole data set to calculate this value, whilst the laser flash equipment only uses the time to half rise, as described in section 2.3.3. Whilst the TherMOL value is offset from the laser flash value (just outside the 4% reported uncertainty value), it does follow the trend very closely. The offset is believed to be due to errors in the Cp value used, as they are based on P91 data, and uncertainties regarding the heat flux used.

Having now established values for the heat flux, thermal diffusivity and the specific heat capacity for the specimen at the test temperature, the thermal conductivity can be calculated. An example of the TherMOL fit to the laser flash data for un-oxidised P92 at 122 °C is presented in Figure 15.

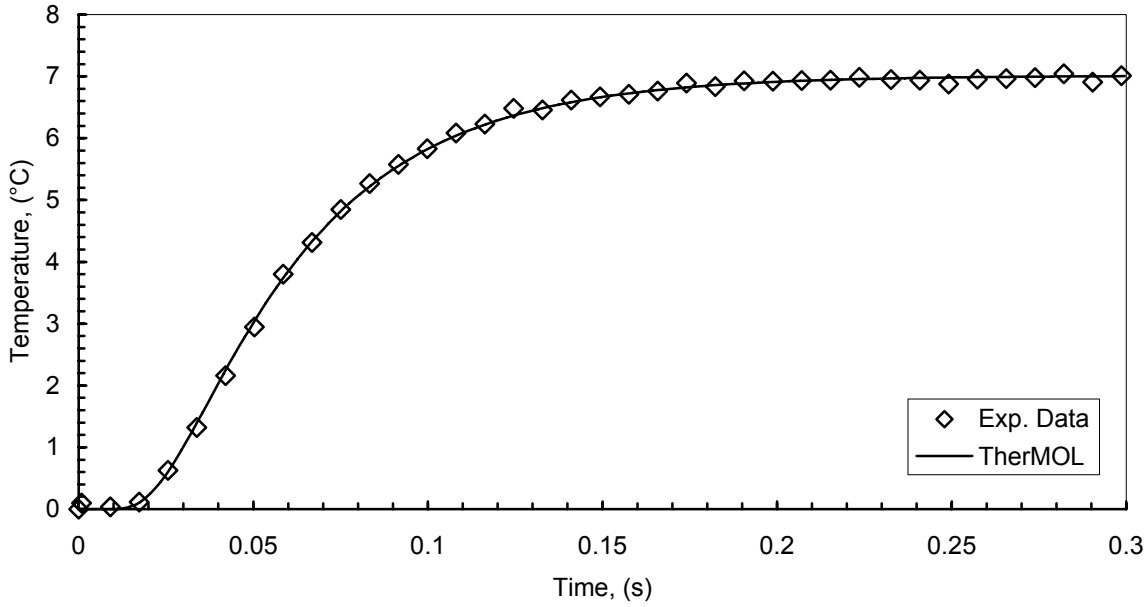

Figure 15 TherMOL fitted curve and experimental data for the temperature rise of P92 at 122 °C

(Numerically fitted values: Heat Flux = 56.1×10^6 W/m^2, λ = 28.9 W/m/K, $\alpha = 7.73 \times 10^{-6}$ W/m^2/K)

Figure 16 and Table 5 show the relationship of thermal conductivity and temperature for P92. For the purposes of this report changes in the density of the material have been ignored.

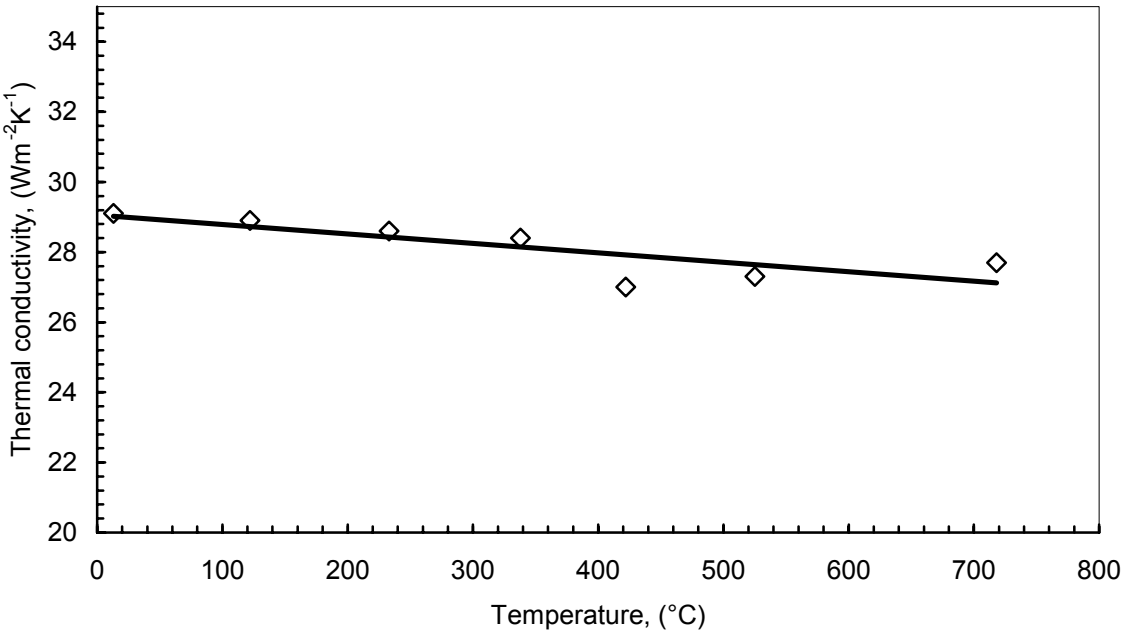

Figure 16 Fitted thermal conductivity values for P92 using TherMOL

Table 5 Thermal property values for P92

Temperature	Cp*	Density*	Thermal Conductivity	Thermal Diffusivity $x10^{-6}$	Heat Flux $x10^{7}$	Time
(°C)	($Jkg^{-1}K^{-1}$)	(kgm^{-3})	($Wm^{-2}K^{-1}$)	(m^2s^{-1})	(Wm^{-2})	(s)
13	442	7770	29.1	8.47	0.62	0.0012
122	481	7770	28.9	7.73	5.61	0.0008
233	519	7770	28.6	7.09	8.88	0.0012
338	551	7770	28.4	6.63	5.80	0.0008
422	581	7770	27.3	6.05	5.31	0.0012
525	641	7770	27.3	5.48	6.11	0.0008
718	930	7770	27.7	3.83	2.90	0.0008

* Ref. 8

4.2.3 Model Calculations for Steam Grown Oxide Scale on P92

Steam oxidised P92 as detailed in section 3, was analysed using the TherMOL model, using the thermal properties for P92 established previously and shown in Table 5. For the purposes of this demonstration the magnetite and spinel layers have been treated as one, and we have assumed a constant density in the absence of measured data. By analysing the laser flash data with TherMOL the thermal diffusivity and the thermal conductivity of the oxide scale layer can be calculated. Figure 17 shows the TherMOL fit to the experimental data for the material parameters presented in Table 6.

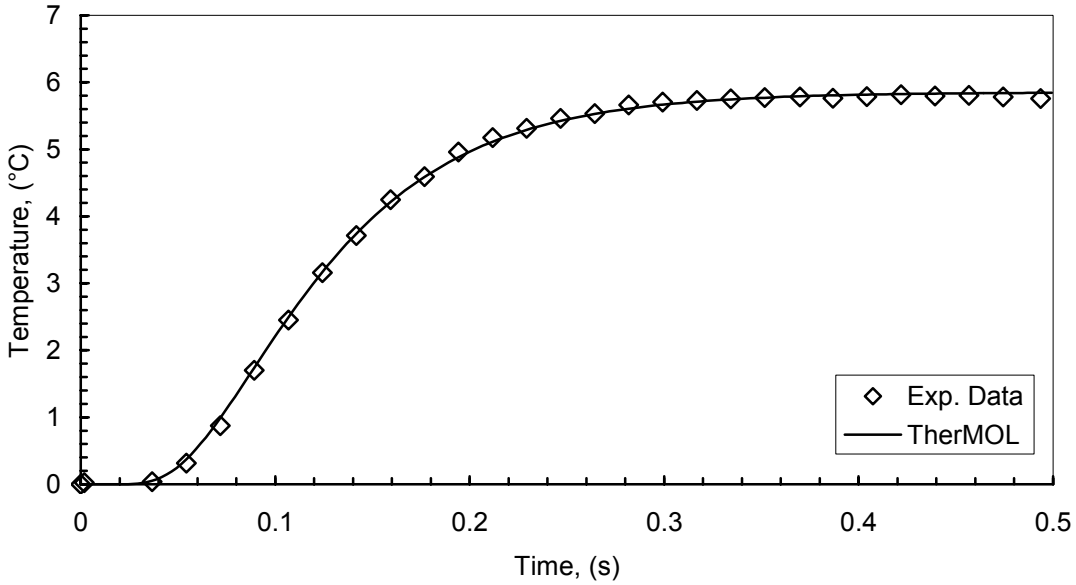

Figure 17 TherMOL fitted curve and experimental data for the temperature rise of P92 and steam grown oxide scale at 205 °C

Table 6 Input parameters for a steam grown oxide scale on P92 at 205 °C.

		P92	Oxide Scale	Units
Properties	Thermal Conductivity	27.77	***0.93***	$Wm^{-2}K^{-1}$
	Density	7770*	5010†	Kgm^{-3}
	Specific Heat	498*	750†	$Jkg^{-1}K^{-1}$
	Thermal Diffusivity	***7.18x10^{-6}***	***2.44x10^{-7}***	m^2s^{-1}
Dimensions	Diameter	0.01262	0.01262	m
	Thickness	0.00186	0.00014	m
	Area	0.000121934	0.000121934	m^2
Flux Parameters	Heat Flux	***3.17x10^{+7}***		Wm^{-2}
	Duration	0.0012		s

* Ref 8.
† Ref 9.
Note: The values in bold italics are fitted values from TherMOL.

Since both the specific heat capacity and density vary with temperature the model required these values for each measurement. The values used are presented in Table 7 along with the predicted thermal conductivity for the oxide scale. Once again the magnetite and spinel layers have been treated as a single layer, using the average value of specific heat. For this demonstration the value of the density used has been kept constant over the whole temperature range.

Table 7 Thermal properties of P92 substrate and oxide scale at different temperatures.

	P92 Substrate		Magnetite	Spinel	Oxide Scale	
Temperature (°C)	Specific Heat Capacity, Cp ($Jkg^{-1}K^{-1}$)*	Thermal Conductivity ($Wm^{-2}K^{-1}$)	Specific Heat Capacity, Cp ($Jkg^{-1}K^{-1}$)†	Specific Heat Capacity, Cp ($Jkg^{-1}K^{-1}$)†	Specific Heat Capacity, Cp ($Jkg^{-1}K^{-1}$)‡	Thermal Conductivity ($Wm^{-2}K^{-1}$)
110	472	28.02	730	658	694	0.934
205	498	27.77	806	695	750	0.915
334	556	27.42	880	725	802	0.925
431	618	27.16	926	741	833	0.851
521	689	26.91	965	754	859	0.766
625	786	26.63	1007	768	887	0.867

* Ref 8 † Ref 10 ‡ Average value of magnetite and spinel

Comparing the values obtained from the model to published values from Armit et al. [13] it is clear that the values obtained through the modelling with TherMOL agree well as shown in Figure 18, where the values differ by approximately 0.5 $Wm^{-2}K^{-1}$. These values show that the TherMOL model can be used successfully to measure the thermal conductivity of multi-layered materials, and that with more detailed measurements of physical and thermal properties, such as density, expansion and Cp, accurate predictions of thermal conductivity can be obtained.

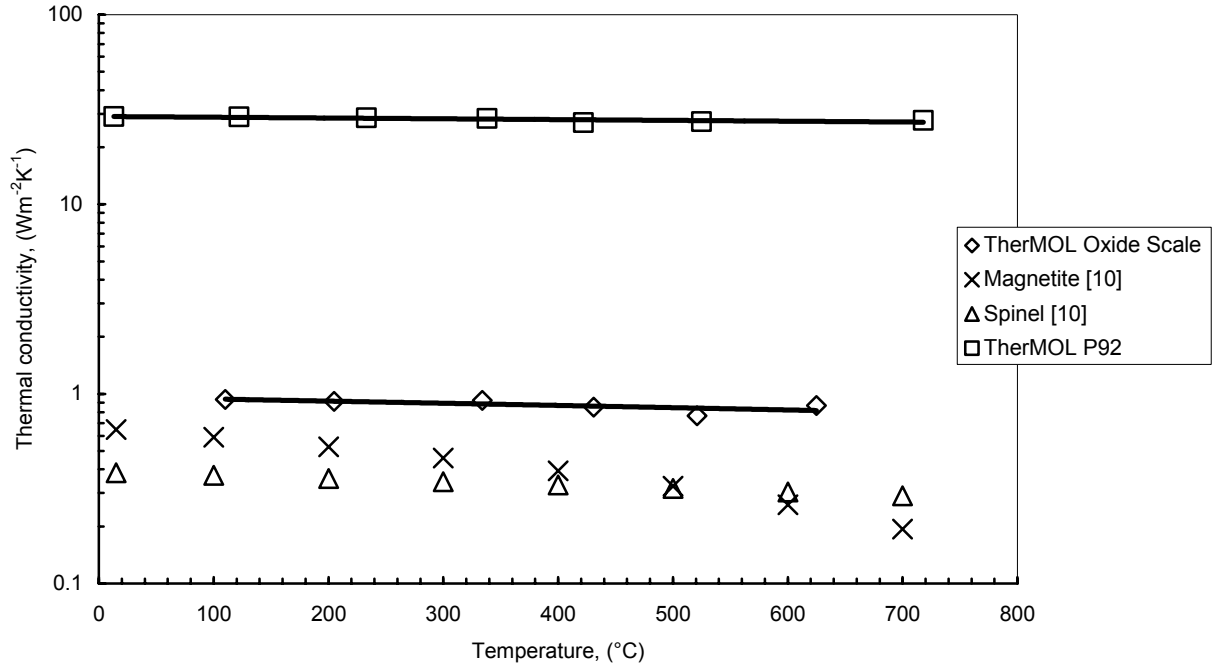

Figure 18 Fitted thermal conductivity values for an oxide scale grown in flowing steam at 650 °C for 200 hours and the P92 substrate on which the oxide was grown.

SUMMARY AND FURTHER WORK

This report has summarised how data obtained from the laser flash technique can be used in conjunction with finite difference modelling to evaluate the thermal diffusivity and conductivity of homogeneous single layer materials and multi-layered/coated materials. Using basic data reported from the laser flash test the following has been demonstrated:

- That the finite difference model TherMOL can simulate the heat transfer through a homogeneous and a multi-layered material.

- Thermal diffusivity calculated from the TherMOL model agrees well with the calculated thermal diffusivity from the commercial laser flash software. The shift seen in Figure 14 could be attributable to several factors, these include temperature calibration of the laser flash equipment, errors in the heat flux used in the model, errors from using only room temperature density in the model and not accounting for expansion in the material under test.

- The model has also been shown to calculate the thermal conductivity for monolithic materials accurately, for example the copper disc, and for multi-layered materials, such as the oxide scale on the P92 substrate. In this instance the model values are very close to calculated values from the literature [13].

- By performing tests and analysing the data over a range of temperatures, simple equations to show the temperature dependency of thermal diffusivity and conductivity can be formulated as shown in Table 8.

Table 8 Temperature dependency of P92 and an oxide scale consisting of magnetite and an iron/chromium spinel, grown in flowing steam at 650 °C for 200 hours.

Property	Material	Relationship with temperature, x (°C)	Linear regression, R^2
Thermal Diffusivity (m^2s^{-1})	P92	$y = -6\times10^{-9}x + 9\times10^{-6}$	0.9904
	Oxide Scale (magnetite + iron/chromium spinel)	$y = -2\times10^{-10}x + 3\times10^{-7}$	0.8782
Thermal Conductivity ($Wm^{-2}K^{-1}$)	P92	$y = -2.7\times10^{-3}x + 29.058$	0.6414
	Oxide Scale (magnetite + iron/chromium spinel)	$y = -2\times10^{-4}x + 0.9627$	0.5068

To progress this method of thermal conductivity measurement further work is required. Within this demonstration we have not considered the effect of thermal expansion or the temperature dependency of density. To improve the accuracy of both the laser flash and the modelling, measurements of the following thermo physical properties should be made and applied to the laser flash analysis and modelling as appropriate.

1. The thermal expansion of the test piece should be measured or calculated from existing data and corrections applied to the laser flash and modelling analysis.

2. The laser flash data should be corrected for errors in the temperature calibration.

3. Control and measurements of the heat flux would remove uncertainties in the modelling stages.

4. Accurate measurement of the specific heat capacity for all the components being measured. This would ideally be performed in a single pan calorimeter so that the Cp measured is under steady state and not transient conditions.

Acknowledgements

This work was carried out under the Lifetime Performance of Materials Programme, a programme of underpinning research funded by the United Kingdom Department of Trade and Industry. The authors are grateful to Mr M U Sheriff, who carried out the steam exposures and metallographic preparation and measurements.

REFERENCES

[1] Parker, Jenkin, Butler, Abbott; J. Appl. Phys., 1961, 32, 1679.
[2] Taylor, Clark; High Temp. - High Press., 1974, 6, 65.
[3] Cowan; J. Appl. Phys., 1963, 34, 926.
[4] Clark, Taylor; J. Appl. Phys., 1975, 46, 714.
[5] Dusza; High Temp. - High Press., 1995/1996, 27/28, 467.
[6] BIPM, IEC, IFCC, ISO, IUPAC, OIML, "Guide to the expression of uncertainty in measurement". International Organisation for Standardisation, Geneva, Switzerland, ISBN 92-67-10188-9, First Edition, 1993 (This Guide is often referred to as the GUM).
[7] Nelder and Mead; (1965), "A simplex method for function minimization", J. Comput., Vol. 7, pp. 308-313.
[8] Powell; "A fast algorithm for nonlinearly constrained optimization calculations", Numerical Analysis, Dundee 1977, Lecture Notes in Mathematics 630, ed. G.A. Watson, Springer-Verlag (Berlin), pp. 144-157.
[9] Fourier; "Théorie Analytique de la Chaleur"(1822) English Translation by A Freeman, Dover Publ., New York, 1955.
[10] Incropera and De Witt; "Fundamentals of Heat and Mass Transfer", John Wiley and Sons, Third Edition, 1981.
[11] Duncan, Urquhart and Roberts, "Review of Measurement and Modelling of Permeation and Diffusion in Polymers – Appendix 1", NPL Report DEPC MPR 012, January 2005.
[12] The T91/P91 Book, Vallourec & Mannesmann Tubes, 1999.
[13] Armitt et al, "The Spalling of Steam-Grown Oxide From Superheater and Reheater Tube Steels". EPRI report February 1978.
[14] Klemme et al., "The heat capacity of MgCr2O4, FeCr2O4, and Cr2O3 at low temperatures and derived thermodynamic properties". American Mineralogist, Vol. 85, 1686-1693, 2000.